LC circuit mediated sympathetic cooling of a proton via image currents

Matthew Bohman (matthew.bohman@mpi-hd.mpg.de)
Max-Planck-Institut für Kernphysik https://orcid.org/0000-0003-1322-1489

Valentin Grunhofer
Johannes Gutenberg University

Christian Smorra
RIKEN https://orcid.org/0000-0001-5584-7960

Markus Wiesinger
Max-Planck-Institut for Nuclear Physics

Christian Will
Max-Planck-Institut for Nuclear Physics

Matthias Borchert
IQO-Hannover

Jack Devlin
RIKEN

Stefan Erlewein
CERN

Markus Fleck
RIKEN https://orcid.org/0000-0003-4114-1902

Steffen Gavranovic
Institut für Physik, Johannes Gutenberg-Universität

James Harrington
MPI-K

Barbara Latacz
RIKEN https://orcid.org/0000-0003-2320-1713

Andreas Mooser
Max-Planck-Institut for Nuclear Physics

Daniel Popper
Institut für Physik, Johannes Gutenberg-Universität

Elise Wursten
CERN

Klaus Blaum
Max-Planck-Institut für Kernphysik https://orcid.org/0000-0003-4468-9316

Yasuyuki Matsuda

University of Tokyo https://orcid.org/0000-0002-9847-3791
Christian Ospelkaus
Leibniz Universität Hannover https://orcid.org/0000-0002-4170-2936
Wolfgang Quint
4GSI Helmholtzzentrum für Schwerionenforschung GmbH
Jochen Walz
University of Mainz
Stefan Ulmer
RIKEN https://orcid.org/0000-0002-4185-4147

Physical Sciences - Article

Keywords: Efficient cooling, trapped charged particles, superconducting LC circuit, proton, image currents

Posted Date: March 24th, 2021

DOI: https://doi.org/10.21203/rs.3.rs-351267/v1

Version of Record: A version of this preprint was published at Nature on August 25th, 2021. See the published version at https://doi.org/10.1038/s41586-021-03784-w.

LC circuit mediated sympathetic cooling of a proton via image currents

M. Bohman,[1,2,*] V. Grunhofer,[3] C. Smorra,[2,3] M. Wiesinger,[1,2] C. Will,[1] M. J. Borchert,[2,4,5] J. A. Devlin,[2,6] S. Erlewein,[2,6] M. Fleck,[2] S. Gavranovic,[3] J. Harrington,[1,2] B. Latacz,[2] A. Mooser,[1] D. Popper,[3] E. Wursten,[2,6] K. Blaum,[1] Y. Matsuda,[7] C. Ospelkaus,[4,5] W. Quint,[8] J. Walz,[3,9] and S. Ulmer[2]
(BASE Collaboration)

[1] *Max-Planck-Institut für Kernphysik, Saupfercheckweg 1, D-69117 Heidelberg, Germany*
[2] *RIKEN, Fundamental Symmetries Laboratory, 2-1 Hirosawa, Wako, Saitama 351-0198, Japan*
[3] *Institut für Physik, Johannes Gutenberg-Universität, Staudingerweg 7, D-55128 Mainz, Germany*
[4] *Institut für Quantenoptik, Leibniz Universität Hannover, D-30167 Hannover, Germany*
[5] *Physikalisch-Technische Bundesanstalt, D-38116 Braunschweig, Germany*
[6] *CERN, 1211 Geneva, Switzerland*
[7] *Graduate School of Arts and Sciences, University of Tokyo, Tokyo 153-8902, Japan*
[8] *GSI Helmholtzzentrum für Schwerionenforschung GmbH, D-64291 Darmstadt, Germany*
[9] *Helmholtz-Institut Mainz, D-55099 Mainz, Germany*

(Dated: March 23, 2021)

Efficient cooling of trapped charged particles is essential in many fundamental physics experiments [1, 2], for high-precision metrology [3, 4], and for quantum technology [5, 6]. Until now, ion-ion coupling for sympathetic cooling or quantum state control has been limited to ion species with accessible optical transitions or has required close-range Coulomb interactions [7, 8]. To overcome this limitation and further develop scalable quantum control techniques, there has been a sustained desire to extend laser-cooling techniques to particles in macroscopically separated traps [5, 9, 10], opening quantum control techniques to previously inaccessible particles such as highly charged ions, molecular ions, and antimatter particles. Here, we demonstrate sympathetic cooling of a single proton by laser cooled Be^+ ions stored in a spatially separated Penning trap. The two traps are connected by a superconducting LC circuit that enables energy exchange over a distance of 9 cm. We simultaneously demonstrate the cooling of a resonant mode of a macroscopic LC circuit with laser-cooled ions and sympathetic cooling of an individually trapped proton, reaching temperatures far below the environment temperature. Importantly, as this technique does not rely on the direct Coulomb interaction but rather on image-current interactions, it can be easily applied to an experiment with antiprotons [1], facilitating improved precision in matter-antimatter comparisons [11] and dark matter searches [12, 13].

Comparisons of fundamental matter-antimatter properties provide stringent constraints on possible violations of the charge-parity-time reversal symmetry and aim to explain the observed overabundance of matter to antimatter in the universe [14]. Measurements of the charge-to-mass ratio and g-factor of the proton and antiproton, a prominent, stable particle-antiparticle system, are limited by cryogenic particle temperatures [15–17] but unlike atomic systems, protons and antiprotons have no electronic structure and are not amenable to standard laser cooling techniques. Moreover, easily laser coolable ions are not readily trapped in the same potential well as negatively charged antiprotons or more exotic forms of antimatter such as the antihydrogen molecular ion, $\bar{H}_2^-$ [18]. Sympathetic laser cooling has been proposed using exotic negatively charged ions [19–21] and via the Coulomb interaction in microscopically separated potentials [1, 22, 23]. Another technique was proposed over thirty years ago to extend laser cooling to antimatter and other exotic systems by coupling to ions with a well-suited cooling transition via ion-induced image currents in trap electrodes [9]. In other contexts, coupling of laser addressable ions to systems with no optical structure has also long been desired for precision spectroscopy [24, 25], mass measurements [26], quantum information [10], and the realisation of novel quantum systems [5].

We have demonstrated the first sympathetic cooling of a single proton by extending the image current coupling technique through the use of a superconducting LC circuit that resonantly enhances the energy exchange between the proton and the laser-cooled ions. Our implementation, illustrated in Fig. 1 a), uses a cryogenic multi-Penning-trap system to store a single proton in the proton trap (PT) and a cloud of Be^+ ions in a separate beryllium trap (BT). The traps confine the particles by a homogeneous magnetic field $\mathbf{B}$ parallel to the electrode centre axis, and an electric quadrupole field with trapping voltage V_0. The motion of the trapped particles is composed of the circular magnetron and modified cyclotron modes in the radial plane, and the harmonic axial mode, at frequencies ν_-, ν_+ and ν_z, respectively [27]. Both traps are realised with a stack of cylindrical electrodes and are separated axially by around 9 cm. LC resonators with a high quality factor (in our case $Q \sim 15\,000$) are commonly used for

* matthew.bohman@mpi-hd.mpg.de

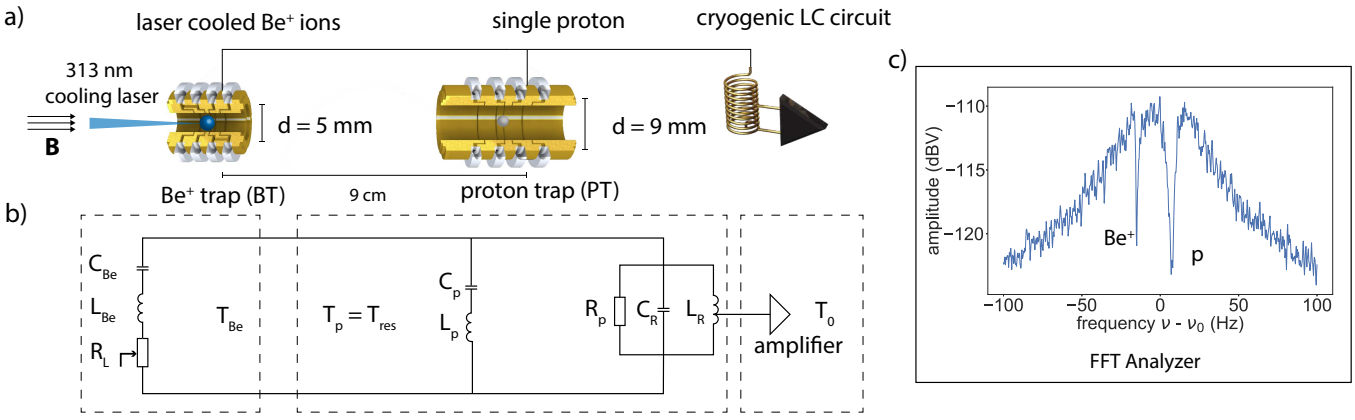

FIG. 1: **a)** A single proton is stored in the proton trap (PT) while one or more Be^+ ion(s) are stored in the beryllium trap (BT). The two ion traps, with inner diameters $d = 9\,\text{mm}$ and $d = 5\,\text{mm}$, respectively, are connected to a cryogenic LC circuit with resonance frequency near their axial frequencies. One end of the resonance circuit is connected to a cryogenic amplifier while the other is connected to rf ground. **b)** This system is described by a three part equivalent circuit, two series LC-circuits representing the trapped particles, and the LC-resonator with effective parallel resistance R_p as parallel RLC-circuit. The amplifier is used to read out the image-current signal of the circuit, and drives the system with voltage noise at an effective temperature T_0. **c)** The resulting FFT spectrum consists of the broad resonance of the detector ($\sim 40\,\text{Hz}$ FWHM) and two narrow "dips" ($\sim 0.8\,\text{Hz}$ FWHM for a single Be^+ ion and $\sim 2.6\,\text{Hz}$ FWHM for the proton) at the axial oscillation frequencies of the two trapped-ion systems.

detection of image currents from the trapped particles [28] and in our experiments we connect the resonator to both traps as shown in Fig. 1 a) so that the two ion-trap systems are coupled via image currents. The LC-circuit with total capacitance $C_R \approx 36\,\text{pF}$ and inductance $L_R \approx 3.0\,\text{mH}$ has an equivalent parallel resistance, at resonance frequency ν_0, of $R_p = 2\pi\,\nu_0\,L_R\,Q$. Illustrated in Fig. 1 b), the entire system is modelled by an equivalent circuit in which the proton and Be^+ ions are series LC circuits with capacitances and inductances C_p, C_{Be}, L_p, and L_{Be} [29] connected in parallel to the superconducting LC circuit. The motion of the Be^+ ions is also damped by the cooling laser, represented as a variable virtual resistance R_L [9]. In contrast to the original sympathetic cooling proposal in which energy is exchanged between the ion-trap systems via a shared electrode [9], we use the LC-circuit resonator to couple the axial modes of the trapped particles. On resonance, the large inductance of the resonator coil compensates the capacitance of the coupling electrode and enhances the ion-induced image current by the Q-value. With the mechanically machined traps used for precision Penning-trap experiments, the $\sim 10\,\text{mHz}$ coupling rates expected from the non-resonant proposal [11] require cooling duty cycles on the scale of minutes and are limited by decoherence, e. g. from voltage fluctuations of the trapping potential. For the parameters used in our resonant cooling demonstration, energy is exchanged between the proton and the sympathetically laser cooled resonator at a rate of 2.6 Hz so that thermal equilibrium is reached after a few seconds and the axial frequencies of the two species can be easily matched. Importantly, by coupling the ion-trap systems via the resonator, the coupling does not rely on a shared electrode so the energy exchange rate is not limited by the trap capacitance. Consequently this cooling scheme can be realised over long distances and with several distributed ion traps.

The noise spectrum of this coupled system is shown in Fig. 1 c) which shows a fast Fourier transform (FFT) of the voltage signal of the resonator. In the absence of additional interactions, the entire system is driven by a combination of the Johnson noise of the resonator and additional voltage noise from the cryogenic amplifier resulting in an effective noise temperature $T_0 = 17.0(2.4)\,\text{K}$. Here, the axial frequencies of the proton in the PT and the Be^+ ion in the BT were set close to resonance with the LC circuit by adjusting the voltage of the axial potential in each trap, $\nu_z \propto V_0^{1/2}$. In the measured noise spectrum, the detector appears as a broad $\sim 40\,\text{Hz}$ (FWHM) resonance while the proton and the Be^+ ions short the parallel resistance of the resonator and appear as narrow dips [29].

We demonstrate that the proton, Be^+ ion(s), and resonator form a system of three coupled oscillators by measuring the noise spectrum at thermal equilibrium. We detune both ion species around three resonator linewidths away from the LC-circuit resonance frequency ν_0 to observe coupling signatures via the FFT lineshape. In these measurements we store the proton in the PT at constant axial frequency and gradually increase the axial frequency of a single Be^+ ion in the BT. Fig. 2 a) shows the resulting FFT spectra, where we observe particle fre-

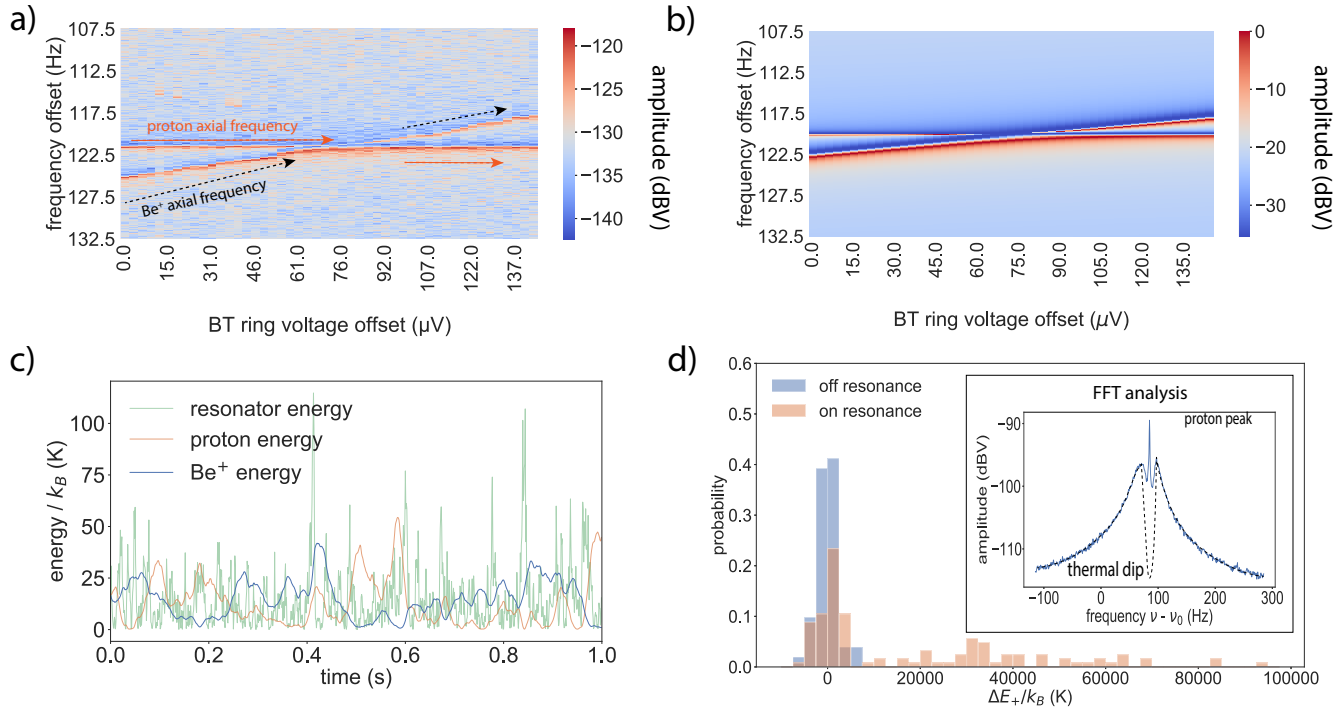

FIG. 2: **a)** Measured FFT spectra of a single Be^+ ion and the proton are presented as vertical cuts of the heatmap. The axial frequency of the proton is fixed and the ring voltage of the BT trapping potential is scanned one step upwards after each FFT is recorded. **b)** The noise spectra expected from the impedance $Z(\nu)$ of the equivalent circuit in Fig. 1 b) are presented in the same way as in a) and are calculated using the same parameters as in the experiment. **c)** An example of the energy exchange between the three oscillators at the resonance frequency of the LC circuit is simulated and includes the energy fluctuations from environment noise of the system. The energy of each oscillator depends on the phase relation with the environment noise so the time series shown here is one of infinitely many that could produce an FFT spectrum used in Fig. 2a). **d)** The change in axial energy of the proton after coupling to the rf-excited Be^+ ions is shown when the Be^+ ions are tuned away from resonance (blue) and tuned to resonance (orange). In both cases the excitation drive is present but only excites the proton via the resonant Be^+ ions. A typical FFT spectrum (inset) shows the excited proton which appears as a narrow peak on top of the resonator and the Be^+ dip which has reduced signal-to-noise compared to thermal equilibrium.

quencies at the dip positions in dark blue, and two of the normal modes of the coupled three oscillator system at the maxima in red. Near the p-Be^+ resonance, the axial motion of both particles is no longer determined by the trapping potential alone, and we observe the coupling signature as an avoided crossing in the normal modes. This feature is consistent with the analytic solution derived from the impedance of the circuit model in Fig. 2 b) (see the methods section) and appears when the three oscillators exchange energy. Using simulations described in the methods section, we show the corresponding time domain behaviour in presence of the environment noise - see Fig. 2 c). In the absence of environmental noise, the energy of each oscillator as a function of time is deterministic and can be found from the initial phases and energy exchange rates. With environmental noise included, energy is still exchanged and, as shown here when laser cooling is absent, the oscillator energies are determined by this equivalent noise temperature.

We further demonstrate that the temperature of the proton can be modified by coupling to a cloud of excited Be^+ ions, typically consisting of around 15 ions. To this end, we apply a parametric rf drive at $2\nu_0$ in the BT, which excites the Be^+ ions if $\nu_{z,Be} = \nu_0$ but, as confirmed by background measurements, has no direct effect on the proton in the PT. By bringing the proton into resonance with the weakly excited Be^+ ions, we produce the characteristic frequency spectrum of the inset of Fig. 2 d) in which the Be^+ ions appear as a broad, shallow dip and the sympathetically excited proton appears as a narrow peak. To quantify the energy transferred to the proton, we measure the axial frequency of the proton before and after coupling to the excited Be^+ ions. Coupling the excited axial mode to the cyclotron mode with a sideband drive at $\nu_+ - \nu_z$ transfers the energy of the axial mode to the cyclotron mode with resulting energy $E_+ = (\nu_+/\nu_z)\, E_z$ [30]. Similar to the continuous Stern-Gerlach effect [31], the quadratic component of the magnetic field in the

PT, $B_2 = -0.39(11)\mathrm{T/m}^2$, interacts with the magnetic moment of the modified cyclotron mode at energy $E_{+,p}$, producing the axial frequency shift $\Delta\nu_z \propto B_2\,\Delta E_{+,p}$ (see the methods section), which we measure to determine the increase in axial energy of the proton. Presented in orange in Fig. 2 d) we show a clear increase of the energy of the proton due to the Be^+ ions and, for background, compare to a measurement in which the Be^+ ions are tuned away from resonance, shown in blue. We see that the energy distribution of the proton is modified by the excited Be^+ ions and acquires a high energy tail with over 40 % of the measured data points outside the 5σ width of the background.

Our demonstration of sympathetic cooling employs similar axial frequency shift measurements in the presence of a continuously laser cooled Be^+ ion cloud. The Be^+ ions are cooled with the closed $^2S_{1/2} \rightarrow {}^2P_{3/2}$ transition [32] and tuned to resonance with the superconducting circuit and the proton, shown in Fig. 3 a). The cooling laser damps the axial motion, increasing the equivalent resistance R_L in Fig. 1 b) and reducing the signal of the broad Be^+ dip. The laser cooled ions reduce the effective noise temperature in the entire circuit and lower the temperature in a narrow frequency range. Using the narrow proton dip as a temperature sensor for the cooled common mode of the system we determine the temperature reduction experimentally with well understood energy dependent shifts of the axial dip and develop further insight into the cooling using time-domain simulations.

A symmetric, cylindrical Penning trap provides a high degree of control over the trapping potential. We use a deliberately introduced trap anharmonicity in the PT which shifts the axial frequency by

$$\delta\nu_z\,(\mathrm{TR}, T) = \frac{1}{4\pi^2 m\nu_z}\frac{3}{2}\frac{C_4\,(\mathrm{TR})}{C_2\,(\mathrm{TR})}\,k_B\,T. \qquad (1)$$

Here, $C_n\,(\mathrm{TR})$ are the coefficients of the expansion of the local trapping potential along the trap axis that depend on the ratio of voltages applied to the central ring electrode (V_0), and the two nearest correction electrodes (V_{CE}), [27, 33, 34], referred to as the tuning ratio, $\mathrm{TR} = V_{\mathrm{CE}}/V_0$. When the laser cooled Be^+ ions are tuned to resonance, the noise energy of the common mode of the proton, resonator, and Be^+ ions is reduced from the noise temperature of the environment resulting in an axial frequency shift,

$$\Delta\nu_z(T_0, T_p, \Delta\mathrm{TR}) = \nu_{z,1}(\mathrm{TR}, T_0) - \nu_{z,2}(\mathrm{TR}, T_p) \qquad (2)$$
$$= \kappa\,\Delta\mathrm{TR} \times (T_0 - T_p), \qquad (3)$$

where $\nu_{z,1}(\mathrm{TR}, T_0) = \nu_z + \delta\nu_z(\mathrm{TR}, T_0)$ is the axial frequency measured at T_0 when the Be^+ ions are detuned and $\nu_{z,2}(\mathrm{TR}, T_p) = \nu_z + \delta\nu_z(\mathrm{TR}, T_p)$ is the axial frequency measured when laser cooled ions are in resonance and reduce the temperature to T_p. The trap anharmonicity is characterised by an offset from the ideal tuning ratio $\Delta\mathrm{TR} = \mathrm{TR} - \mathrm{TR}(C_4 = 0)$ and a constant determined from the trap geometry $\kappa = 45.4\,\mathrm{Hz/K}$ that we crosscheck with additional measurements that use electronic feedback to change the temperature of the resonator. We measure $\Delta\nu_z$ as a function of $\Delta\mathrm{TR}$ and the measured slope s determines the change in temperature, $\Delta T = T_0 - T_p = -s/\kappa$. The results of an example measurement are shown in blue in Fig. 3 b). With 10 Be^+ ions in resonance we measure a slope $s = -350\,(14)\,\mathrm{Hz}$ and in a background measurement with the Be^+ ions detuned, shown in orange, obtain a slope $s = 4\,(13)\,\mathrm{Hz}$. This corresponds to a temperature reduction of $\Delta T = 7.7\,(0.3)\,\mathrm{K}$ and is the first demonstration of sympathetic laser cooling of a single trapped proton. With a significance of more than 20 standard deviations, this also constitutes the first demonstration of remote, image current mediated sympathetic cooling, applicable to any charged particle without convenient cooling transitions.

The temperature of the proton is determined by the noise power dissipated by the laser cooled ions. In the circuit representation, increasing the damping of the laser cooling γ_L increases R_L and has the effect of lowering the coupling rate of the Be^+ ions to the resonator $\widetilde{\gamma}_{\mathrm{Be}}$. In the absence of laser cooling is given by the dip width $\gamma_{\mathrm{Be}} \propto N_{\mathrm{Be}}$. For a given number of laser cooled ions N_{Be}, γ_L must be optimised and in the limiting case when $\gamma_L \ll \gamma_{\mathrm{Be}}$ the Be^+ ions are driven by the resonator and the dip signal is unchanged. Likewise when $\gamma_L \gg \gamma_{\mathrm{Be}}$, the Be^+ ions are decoupled from the resonator and the dip signal vanishes. In both limiting cases, the temperature of the resonator and the proton remains unchanged.

However, increasing N_{Be} increases $\widetilde{\gamma}_{\mathrm{Be}}$ and laser cooling reduces the temperature of the resonator and the proton, even at large γ_L. To lower the temperature and to investigate the scaling of T_p, we performed a series of further measurements with varying N_{Be} and laser detuning δ shown in Fig. 4. We additionally analysed the temperature scaling by comparing to a temperature model in which the common mode temperature T_{CM} of the equivalent circuit is arises from competing dissipation sources - the noise temperature of the environment, T_0, at a coupling rate given by the width of the LC resonance γ_D, and to the Be^+ ions at temperature T_{Be}. As a result, the system comes to thermal equilibrium at

$$T_p = T_{\mathrm{CM}} \qquad (4)$$
$$T_{\mathrm{CM}} = \frac{T_0\,\gamma_D + T_{\mathrm{Be}}\,\widetilde{\gamma}_{\mathrm{Be}}}{\gamma_D + \widetilde{\gamma}_{\mathrm{Be}}}. \qquad (5)$$

When $\widetilde{\gamma}_{\mathrm{Be}} \gg \gamma_D$, the proton temperature is approximated as

$$T_p \approx T_0\,\frac{\gamma_D}{\widetilde{\gamma}_{\mathrm{Be}}} + T_{\mathrm{Be}}, \qquad (6)$$

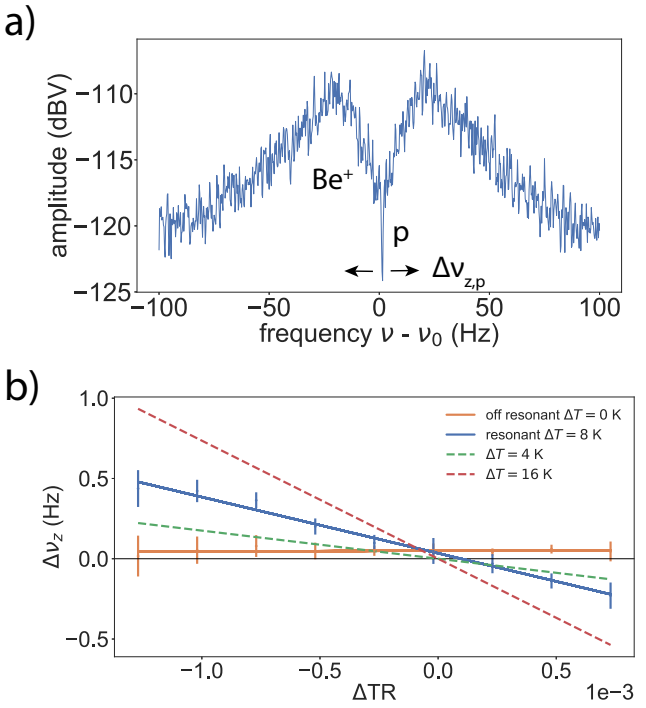

FIG. 3: **a)** A cloud of laser cooled Be^+ ions appears on the resonator as a broad dip that reduces the temperature of that resonator mode. The proton spectral dip is much narrower and continues to short the resonator noise and can be used as a temperature probe via Eq. (3). **b)** A characteristic measurement of ΔT_z is shown for $N_{\mathrm{Be}} \approx 10$ and the laser red detuned by $\delta \approx 100\,\mathrm{MHz}$. Error bars represent the standard deviation of the measured data and the change in temperature is extracted from the slope. Calculated slopes, the red and green dashed lines, illustrate the scaling of the slope with ΔT.

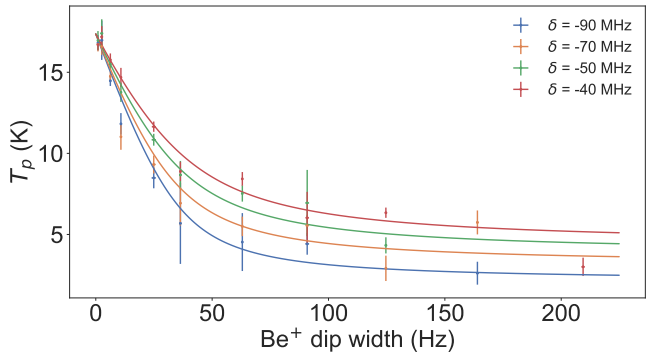

FIG. 4: The temperature of the cooled proton-resonator system is shown as a function of the laser detuning δ and the coupling of the laser cooled Be^+ ions to the resonator parametrized by the dip width. Here, vertical error bars represent the fit uncertainty of the measured slope and the horizontal error bars represent the standard error of γ_{Be}. Fits to the data are shown to illustrate the $1/N_{\mathrm{Be}}$ scaling when the dip width becomes larger than the resonator width - around 40 Hz.

reproducing the $1/N_{\mathrm{Be}}$ scaling, by $\gamma_{\mathrm{Be}} \propto N_{\mathrm{Be}}$, that appears in the non-resonant proposal [9, 11] and related proposals in the context of trapped ion quantum information [10, 35, 36]. The data point for the largest ion cloud $\gamma_{\mathrm{Be}} = 164\,(5)\,\mathrm{Hz}$ and largest detuning from the centre of the cooling transition $\delta = -90\,\mathrm{MHz}$ in Fig. 4 is representative for the lowest temperatures observed in our measurements. Here, we achieve a temperature reduction of

$$\Delta T_p = 14.4\,(0.7)\,\mathrm{K}. \tag{7}$$

The uncertainty of the final temperature of the proton is dominated by the uncertainty of the environment temperature at $T_0 = 17.0(2.4)\,\mathrm{K}$ and we obtain

$$T_p = T_0 - \Delta T_p = 2.6\,(2.5)\,\mathrm{K}, \tag{8}$$

demonstrating a temperature reduction of 85 %.

Lower temperatures can be achieved by lowering the noise temperature of the amplifier, T_0, increasing the Q-value of the resonator, or by operating with smaller traps that increase γ_{Be} quadratically with lower radius. In addition, by performing these demonstration measurements fully on resonance for maximal coupling rates, the balance of heating by the resonator to cooling by the Be^+ ions is maximally inefficient, and future cooling work will be done off-resonantly to balance the coupling rate and the temperature limit with engineered cooling sequences [37].

In the context of our experimental goals, this technique can be readily applied to sympathetically laser cool protons and antiprotons in the same large macroscopic traps that enable precision measurements of the charge-to-mass ratio and g-factor [1, 11]. In measurements of nuclear magnetic moments this will enable nearly 100% spin-flip fidelity [11, 16, 17, 38] and can reduce the dominant systematic effect proportional to the particle temperature in the highest precision mass measurements [39–41]. In addition, this technique can also be used to cool other exotic systems such as highly charged ions [24, 25] or molecular ions [18, 42] for sideband resolved spectroscopy, using only a single cooling laser. The sympathetically cooled resonator can also be used as a sensitivity enhanced probe of new physics, for example in dark matter searches [13, 42, 43]. Most importantly though, this demonstration realises a long sought experimental technique that will enable enhanced precision experiments of any charged species at lower temperatures.

ACKNOWLEDGMENTS

This study comprises parts of the PhD thesis work of M.B. We acknowledge the contributions of G.L. Schneider and N. Schön to the design and construction of the Penning-trap system. We thank Sven Sturm for helpful discussions regarding the cooling method presented here and acknowledge similar developments toward cooling highly charged ions in the ALPHATRAP collaboration. We acknowledge financial support from the RIKEN Chief Scientist Program, RIKEN Pioneering Project Funding, the RIKEN JRA Program, the Max-Planck Society, the Helmholtz-Gemeinschaft, the DFG through SFB 1227 'DQ-mat', the European Union (Marie Skłodowska-Curie grant agreement number 721559), the European Research Council (ERC) under the European Union's Horizon 2020 research and innovation programme (Grant agreement Nos. 832848 - FunI and 852818 - STEP) and the Max-Planck–RIKEN–PTB Center for Time, Constants and Fundamental Symmetries.

AUTHOR CONTRIBUTIONS

M.B., A.M., S.U., J.W. and M.W. designed the experimental apparatus. M.B., A.M., and M.W. assembled the trap and laser systems. M.B., V.G., C.S., and M.W. contributed to the experiment run. M.B. and C.S. implemented the presented methods, recorded and evaluated the presented experiment data. C.W. developed the simulation code and provided the simulation results. M.B., C.S., K.B., and S.U. prepared the manuscript, which was discussed and approved by all authors.

COMPETING INTERESTS

The authors declare no competing interests.

DATA AVAILABILITY

The datasets generated during and/or analysed during this study are available from the corresponding authors on reasonable request.

CODE AVAILABILITY

The code used during during this study are available from the corresponding authors on reasonable request.

I. METHODS

A. Equations of motion for the coupled ion-trap systems

The axial motions of the trapped proton and Be^+ ion(s) are described by a harmonic oscillator driven by the oscillating voltage on the trap electrodes connected to the resonant LC circuit, V_{LC}, and in the case of the Be^+ ion(s) by an additional photon scattering force from the cooling laser, F_L:

$$\begin{aligned} m_p \ddot{z}_p + m_p \omega_{z,p}^2 \, z_p &= \frac{q}{D_p} V_{LC} \\ m_{\mathrm{Be}} \ddot{z}_{\mathrm{Be}} + m_{\mathrm{Be}} \omega_{z,Be}^2 z_{\mathrm{Be}} &= \frac{q}{D_{\mathrm{Be}}} V_{LC} + F_L. \end{aligned} \tag{9}$$

V_{LC} is composed of voltage noise from the environment, V_{noise}, and the voltage arising from image currents induced by the proton and Be^+ ion(s), I_p and I_{Be}, respectively. On resonance $\omega_R = \omega_{z,p} = \omega_{z,Be}$, the impedance of the LC-circuit is given by its equivalent parallel resistance, R_p, and

$$\frac{1}{\omega_R^2} \ddot{V}_{LC} + \frac{1}{Q\,\omega_R} \dot{V}_{LC} + V_{LC} = L_R \left(\dot{I}_{\mathrm{noise}} + \dot{I}_p + \dot{I}_{\mathrm{Be}} \right). \tag{10}$$

I_{noise} is the noise current from the environment, and I_p and I_{Be} are the induced image currents of the proton and the Be^+ ions, respectively:

$$I_{p,Be} = \frac{q}{D_{p,Be}} \dot{z}_{p,Be}, \tag{11}$$

where $D_{p,Be}$ are the trap dependent effective electrode distances [29].

The equations of motion and the equation for the voltage in the LC-circuit form a set of coupled stochastic differential equations without closed analytic solutions available. As a result, we analyse the frequency response of the system by calculating the impedance of the equivalent circuit in Fig. 1 b) and estimate the energy of the proton by calculating the temperatures of each component based on their energy exchange rates. Finally, we numerically integrate the differential equations in simulations that allow the comparison of FFT spectra and the visualisation of the time-domain behaviour in the system.

B. Impedance analysis of the equivalent circuit

The FFT spectrum shown in Fig. 1c) results from the noise on the image current detector $u_n^2 = 4k_B T_0 \,\mathrm{Re}\,[Z(\omega)]\,\Delta f$ at effective noise temperature T_0, FFT bandwidth Δf, and the impedance $Z(\omega)$ of the circuit in Fig. 1 b). The lineshape of resistively cooled particles stored in a single trap based on the impedance of

the equivalent circuit is well understood [29, 44]. Here, we evaluate the impedance for two independently biased ion-trap systems as:

$$\frac{\mathrm{Re}\left[Z(\omega)\right]}{R_p} = \left(1+\frac{k_L}{k_L^2+\delta_{\mathrm{Be}}(\omega)^2}\right)/ \left(\left(1+\frac{k_L}{k_L^2+\delta_{\mathrm{Be}}(\omega)^2}\right)^2+\delta_R(\omega)^2+\delta_p(\omega)^{-2}+ \frac{\delta_{\mathrm{Be}}(\omega)^2}{\left(k_L^2+\delta_{\mathrm{Be}}(\omega)^2\right)^2}-\frac{2\delta_R(\omega)}{\delta_p(\omega)}- \frac{2\delta_R(\omega)\delta_{\mathrm{Be}}(\omega)}{\left(k_L^2+\delta_{\mathrm{Be}}(\omega)^2\right)}+\frac{2\delta_{\mathrm{Be}}(\omega)}{\delta_p(\omega)\left(k_L^2+\delta_{\mathrm{Be}}(\omega)^2\right)}\right), \quad (12)$$

where $k_L = R_L/R_p$ allows for additional damping in one of the traps. The lineshapes of the individual components arise from $\delta_i(\omega) = 2(\omega-\omega_i)/\gamma_i$ which are parameters proportional to the ratio of the frequency detuning $(\omega-\omega_i)$ to the oscillator linewidth, γ_i. The index $i \in \{R, Be, p\}$ corresponds to the resonator, the Be^+ ions, and the proton, respectively. In the absence of additional damping $k_L = 0$ the impedance simplifies to:

$$\frac{\mathrm{Re}\left[Z(\omega)\right]}{R} = \frac{1}{1+\delta_R^2+\delta_p^{-2}+\delta_{\mathrm{Be}}^{-2}-2\frac{\delta_R}{\delta_p}-2\frac{\delta_R}{\delta_{\mathrm{Be}}}+2\frac{1}{\delta_p\delta_{\mathrm{Be}}}}, \quad (13)$$

which describes the lineshape of the data shown in Fig. 1 c). Similarly, the heat maps in Fig. 2 a) and Fig. 2 b) compare the FFT spectra from experiment to ones calculated with $Z(\omega)$, and observe consistent behaviour.

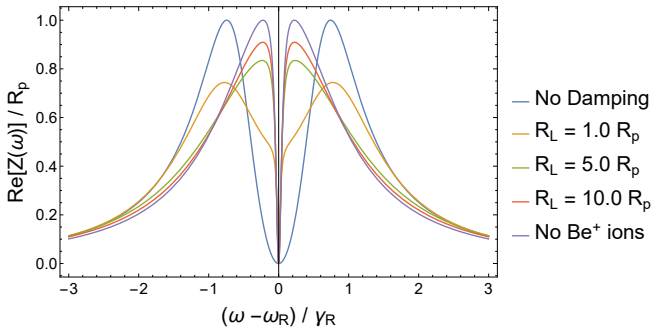

FIG. 5: The normalised impedance $\mathrm{Re}\left[Z(\omega)\right]/R_p$ is plotted for different values of R_L, where no damping corresponds to $R_L = 0$, and no Be^+ ions to $R_L \to \infty$. Here, $\gamma_R = 2\,\gamma_{\mathrm{Be}} = 20\,\gamma_p$, corresponding in experiment to about 30 Be^+ ions and a single proton.

With laser cooling included, $R_L > 0$ and the dip feature of the Be^+ ions is modified as displayed in Fig. 3 a). The corresponding impedance is calculated for varying R_L in Fig. 5. In both cases, regardless of the value of R_L, the proton shorts the noise of the LC-circuit on resonance. As described in the main text, the Be^+ ions decouple from the LC circuit as R_L reduces the fraction of noise power dissipated in the series LC-circuit of the Be^+ ions - ultimately leading to a vanishing dip signal. This decoupling effect is well known from other coupled oscillator systems [45] and motivates the reduced coupling of the Be^+ ions to the LC-circuit, $\widetilde{\gamma}_{\mathrm{Be}} < \gamma_{\mathrm{Be}}$.

C. Temperature Model

The temperature model presented here is described in [46] and assumes that each component of the three oscillator system consisting of the trapped proton, the trapped Be^+ ion(s), and the resonator comes to thermal equilibrium with the rest of the system at temperatures defined by the energy exchange rates in the system.

The Be^+ ions, are damped by the resonator as well as the cooling laser and the power transmitted by the Be^+ ions is then written,

$$\left\langle \frac{dE_{\mathrm{Be}}}{dt} \right\rangle = k_{\mathrm{B}}\, T_{\mathrm{Be}} \widetilde{\gamma}_{\mathrm{Be}} + \left\langle \frac{dE_{\mathrm{Be}}}{dt} \right\rangle_{\mathrm{laser}}, \quad (14)$$

where $\left\langle \frac{dE_{\mathrm{Be}}}{dt} \right\rangle_{\mathrm{laser}}$ is the the power dissipated by scattered photons. An identical analysis applies to the resonator which is coupled to the environment with a coupling rate γ_D given by the width of the resonance, or the Q-value, and to the Be^+ ions with a coupling rate, $\widetilde{\gamma}_{\mathrm{Be}}$. These relations produce the system of equations shown in the main text,

$$T_p = T_{\mathrm{CM}} \quad (15)$$

$$T_{\mathrm{CM}} = \frac{T_0\,\gamma_D + T_{\mathrm{Be}}\,\widetilde{\gamma}_{\mathrm{Be}}}{\gamma_D + \widetilde{\gamma}_{\mathrm{Be}}}. \quad (16)$$

The power dissipated by the resonator while the Be^+ ions are laser cooled can be written as

$$k_B\, T_{\mathrm{CM}}\, \widetilde{\gamma}_{\mathrm{Be}} = \left\langle \widetilde{J}_z \right\rangle R_p, \quad (17)$$

and in combination with the power dissipated by the resonator in the absence of laser cooling,

$$k_B\, T_0\, \gamma_{\mathrm{Be}} = \langle J_z \rangle\, R_p, \quad (18)$$

allows the reduced coupling rate to be written as,

$$\widetilde{\gamma}_{\mathrm{Be}} = \frac{T_0}{T_{\mathrm{CM}}}\, k\, \gamma_{\mathrm{Be}}, \quad (19)$$

where k is defined by the ratio,

$$k = \frac{\left\langle \widetilde{J}_z^2 \right\rangle}{\langle J_z^2 \rangle}. \quad (20)$$

Although k can, in principle, be extracted from the FFT spectrum, the extraction of individual k values is imprecise and k and T_{Be} are treated as constant fit parameters

in Fig. 4. A more accurate determination of $\left\langle \frac{dE_{\mathrm{Be}}}{dt} \right\rangle_{\mathrm{laser}}$ can be performed by measuring the photon scattering rate [9] and is planned for future measurements.

D. Simulations and Time Domain Behaviour

We access the time domain behaviour of the proton-ion-resonator system through simulations, which are performed by numerically integrating Eq. (9) and Eq. (10). By replacing $V_{LC} = L_R \dot{I}_L$, where I_L is the current flowing through the inductance L_R, these equations can be rewritten as,

$$\begin{aligned} m_p \ddot{z}_p + m_p\,\omega_{z,p}^2 z_p &= \frac{q}{D_p} L_R\,\dot{I}_L \\ m_{\mathrm{Be}}\,\ddot{z}_{\mathrm{Be}} + m_{\mathrm{Be}}\,\omega_{z,Be}^2\,z_{\mathrm{Be}} &= \frac{q}{D_{\mathrm{Be}}} L_R\,\dot{I}_L + F_L \\ L_R\,C_R \ddot{I}_L + \frac{L_R}{R_p}\dot{I}_L + I_L + I_{\mathrm{noise}} + \frac{q}{D_p}\dot{z}_p + \frac{q}{D_{\mathrm{Be}}}\dot{z}_{\mathrm{Be}} &= 0. \end{aligned} \tag{21}$$

The integration is performed in time steps of $\Delta t = 1\,\mathrm{ns}$ for most simulations and the equivalent thermal noise $\left\langle I_{\mathrm{noise}}^2 \right\rangle = 4k_B T_0 \Delta f / R_p$ is computed in each step n as

$$I_{\mathrm{noise},n} = \sqrt{2k_b T_0/(R_p \Delta t)} \cdot G_n(\mu = 0, \sigma = 1), \tag{22}$$

where, due to the discrete time steps, the noise bandwidth is defined as $\Delta f = 1/(2\Delta t)$. $G_n(\mu = 0, \sigma = 1)$ is a Gaussian distribution with mean $\mu = 0$ and standard deviation $\sigma = 1$ which is sampled every step, conserving the standard deviation of the noise while fulfilling the criterion that two subsequent values must be uncorrelated.

Laser cooling is implemented as a force F_L resulting from the absorption and emission of individual photons from a cooling laser at frequency $f_0 + \Delta f$, which is red detuned from the centre of the cooling transition at frequency f_0. In each simulation step in which the ion passes the absorption velocity, i.e. $v_{n+1} > v_{abs}$ and $v_n < v_{abs}$, the ion absorbs a photon with probability defined by the laser intensity and receives a momentum kick $\mathbf{\Delta p}$. In the excited state the ion is not allowed to absorb photons and decays to the ground state with probability $\exp\left(\frac{\Delta t}{\tau}\right)$ where τ is the excited state lifetime. Upon decay, the ion receives an axial momentum kick, $p_z = |\mathbf{\Delta p}| \cos(\phi)$, where ϕ is evenly distributed from 0 to 2π to account for the random direction of the emitted photon.

Data preparation and analysis is performed in R [47], while the calculation intensive part is outsourced to C++ via the Rcpp-package [48]. We employ a fourth order symplectic integrator [49] to calculate the particle trajectories and the voltage across the RLC circuit to ensure that energy is, on average, conserved for numeric integration with more than 10^{10} steps.

In simulations of the p-Be^+-resonator system we apply the conditions of the experiments described in the main text to reproduce the frequency domain behaviour, with Fig. 6 a) and Fig. 6 b) corresponding to the experimental results shown in the inset of Fig. 2 d) and Fig. 3 a), respectively. The evolution of the oscillator energies with 10 Be^+ ions, $N_{\mathrm{Be}} = 10$, is shown in Fig. 6 c). Starting from $t = 7.5\,\mathrm{s}$ a parametric drive is applied resulting in a significant increase of the energy of the proton and the Be^+ ions from an initial temperature of 17 K. Similarly, Fig. 6 d) shows the energy exchange between a single proton, a single Be^+ ion, and the resonator all on resonance, where the cooling laser is applied from $t = 10\,\mathrm{s}$, resulting in rapid cooling of the Be^+ ions and a temperature reduction of the proton.

E. Axial Frequency Shifts

A particle in a Penning trap is subjected to shifts of the mode frequencies due to the inhomogeneity of the magnetic field and the anharmonic contributions to trapping potential [27, 34]. The magnetic field in the trap centre can be written with the lowest order corrections as:

$$\mathbf{B}(z, r) = B_0\,\hat{z} + B_2\left(\left(z^2 - r^2/2\right)\hat{z} - r\,z\,\hat{r}\right), \tag{23}$$

where a quadratic gradient B_2 shifts the axial frequency as a function of the radial energy by:

$$\Delta\nu_z = \frac{1}{4\pi^2\,m\,\nu_z}\frac{B_2}{B_0}\,E_+. \tag{24}$$

We use this effect to demonstrate the energy exchange between the heated Be^+ ions and the proton in Fig. 2 c). Here, the proton axial mode and modified cyclotron mode are sideband-coupled with a quadrupolar rf-drive, so that after the sideband coupling the proton cyclotron energy freezes out at an energy $E_+ = (\nu_+/\nu_z)E_z$, where E_z is the axial energy while coupling the axial mode to the excited Be^+ ions.

The proton trap is optimised to have a homogeneous magnetic field and is unsuited for energy measurements using Eq. (24) at low energy, with a temperature resolution of $< 0.1\,\mathrm{mHz/K}$. In the the sympathetic cooling measurements presented here, we instead used the trapping potential anharmoncity that we introduced in the PT to determine the temperature of the trapped particle. The trapping potential can be expanded in terms of C_n coefficients [27, 33, 34], and the higher-order terms C_{2n}, $n \geq 2$ shift the trap frequencies ν_i by

$$\Delta\nu_i \propto C_{2n} E_j^{n-1} \tag{25}$$

where E_j is the energy of a trap mode. The coefficients C_n can be written in terms of a "tuning ratio", TR, defined by the ratio of the voltage applied to the central ring

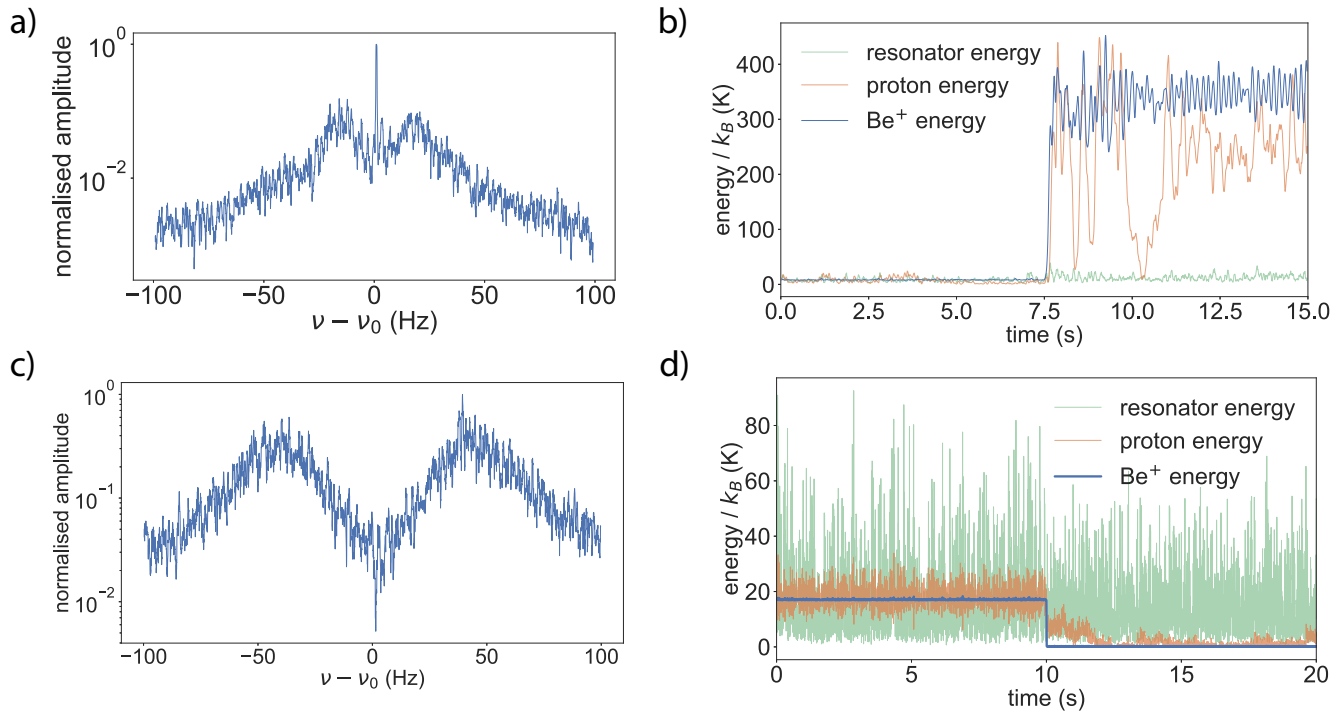

FIG. 6: Computed FFT spectra are given in a) and c) to compare to the experimental results presented in the inset of Fig. 2 d) and Fig. 3 a) in the main text, respectively. In c) and d), we show representative time domain behaviour during heating and cooling measurements where the excitation drive or cooling laser is applied at times $t = 7.5\,\mathrm{s}$ and $t = 10\,\mathrm{s}$, respectively.

electrode to the voltage applied to a correction electrode, as

$$C_n = E_n + D_n\,\mathrm{TR}. \tag{26}$$

D_n can be calculated from the trap geometry and the axial frequency shift due to the leading energy dependent trap anharmonicity C_4 can be written as,

$$\Delta\nu_z = \frac{1}{4\pi^2 m\nu_z}\frac{3}{2}\frac{D_4}{C_2}\,k_B\,T_z\,\Delta\mathrm{TR}, \tag{27}$$

where ΔTR is the offset in applied tuning ratio from the ideal tuning ratio at which $C_4 = 0$. Ultimately the axial frequency shift as a function of TR and the axial energy E_z can be expressed as

$$\Delta\nu_z = \kappa_{D_4} E_z, \tag{28}$$

where, for a proton stored in the PT, $\kappa_{D_4} = 45.4\,\Delta\mathrm{TR\,Hz/K}$. This effect is used to determine the change of the proton axial temperature while the resonator is cooled with the laser-cooled Be$^+$ ions, and is the underlying method for the data shown in Fig. 3 and Fig. 4.

Temperature measurements using this method are limited by the determination of T_0 to the $\sim 1\,\mathrm{K}$ level. We have previously performed higher precision temperature measurements using a dedicated, spatially distant trap with a ferromagnetic ring electrode that uses the shift of Eq. (24) to obtain a cyclotron energy resolution of up to 80 Hz/K [16, 50] and have developed a similar trap to reach 10 mK temperature resolution in future cooling measurements.

[1] C. Smorra, K. Blaum, L. Bojtar, et al. BASE–the baryon antibaryon symmetry experiment. *The European Physical Journal Special Topics*, 224(16):3055–3108, 2015.

[2] S. Sturm, I. Arapoglou, A. Egl, et al. The ALPHATRAP experiment. *The European Physical Journal Special Topics*, 227(13):1425–1491, 2019. doi:10.1140/epjst/e2018-800225-2.

[3] N. Huntemann, C. Sanner, B. Lipphardt, Chr. Tamm, and E. Peik. Single-ion atomic clock with 3×10^{-18} systematic uncertainty. *Phys. Rev. Lett.*, 116:063001, 2016. doi:10.1103/PhysRevLett.116.063001.

[4] S. M. Brewer, J.-S. Chen, A. M. Hankin, et al. $^{27}Al^{+}$ quantum-logic clock with a systematic uncertainty below 10^{-18}. *Phys. Rev. Lett.*, 123:033201, 2019. doi:10.1103/PhysRevLett.123.033201.

[5] S. Kotler, R. W. Simmonds, D. Leibfried, and D. J. Wineland. Hybrid quantum systems with trapped charged particles. *Phys. Rev. A*, 95:022327, 2017. doi:10.1103/PhysRevA.95.022327.

[6] C. D. Bruzewicz, J. Chiaverini, R. McConnell, and J. M. Sage. Trapped-ion quantum computing: Progress and challenges. *Applied Physics Reviews*, 6(2):021314, 2019. doi:10.1063/1.5088164.

[7] K. R. Brown, C. Ospelkaus, Y. Colombe, et al. Coupled quantized mechanical oscillators. *Nature*, 471(7337):196–199, 2011. doi:10.1038/nature09721.

[8] M. Harlander, R. Lechner, M. Brownnutt, R. Blatt, and W. Hänsel. Trapped-ion antennae for the transmission of quantum information. *Nature*, 471(7337):200–203, 2011. doi:10.1038/nature09800.

[9] D. J. Heinzen and D. J. Wineland. Quantum-limited cooling and detection of radio-frequency oscillations by laser-cooled ions. *Physical Review A*, 42(5):2977, 1990.

[10] N. Daniilidis, T. Lee, R. Clark, S. Narayanan, and H. Häffner. Wiring up trapped ions to study aspects of quantum information. *Journal of Physics B: Atomic, Molecular and Optical Physics*, 42(15):154012, 2009. doi:10.1088/0953-4075/42/15/154012.

[11] M. Bohman, A. Mooser, G. Schneider, et al. Sympathetic cooling of protons and antiprotons with a common endcap Penning trap. *Journal of Modern Optics*, 65(5-6):568–576, 2018. doi:10.1080/09500340.2017.1404656.

[12] C. Smorra, Y. V. Stadnik, P. E. Blessing, et al. Direct limits on the interaction of antiprotons with axion-like dark matter. *Nature*, 575(7782):310–314, 2019. doi:10.1038/s41586-019-1727-9.

[13] J. A. Devlin, M. J. Borchert, S. Erlewein, et al. Constraints on the coupling between axionlike dark matter and photons using an antiproton superconducting tuned detection circuit in a cryogenic Penning trap. *Phys. Rev. Lett.*, 126:041301, 2021. doi:10.1103/PhysRevLett.126.041301.

[14] M. Dine and A. Kusenko. Origin of the matter-antimatter asymmetry. *Rev. Mod. Phys.*, 76:1–30, 2003. doi:10.1103/RevModPhys.76.1.

[15] S. Ulmer, C. Smorra, A. Mooser, et al. High-precision comparison of the antiproton-to-proton charge-to-mass ratio. *Nature*, 524(7564):196–199, 2015. doi:10.1038/nature14861.

[16] G. Schneider, A. Mooser, M. Bohman, et al. Double-trap measurement of the proton magnetic moment at 0.3 parts per billion precision. *Science*, 358(6366):1081–1084, 2017. ISSN 0036-8075. doi:10.1126/science.aan0207.

[17] C. Smorra, S. Sellner, M. J. Borchert, et al. A parts-per-billion measurement of the antiproton magnetic moment. *Nature*, 550(7676):371–374, 2017. doi:10.1038/nature24048.

[18] E. G. Myers. *CPT* tests with the antihydrogen molecular ion. *Phys. Rev. A*, 98:010101, 2018. doi:10.1103/PhysRevA.98.010101.

[19] P. Yzombard, M. Hamamda, S. Gerber, M. Doser, and D. Comparat. Laser cooling of molecular anions. *Phys. Rev. Lett.*, 114:213001, 2015. doi:10.1103/PhysRevLett.114.213001.

[20] R. Tang, R. Si, Z. Fei, et al. Candidate for laser cooling of a negative ion: High-resolution photoelectron imaging of Th^{-}. *Phys. Rev. Lett.*, 123:203002, 2019. doi:10.1103/PhysRevLett.123.203002.

[21] G. Cerchiari, P. Yzombard, and A. Kellerbauer. Laser-assisted evaporative cooling of anions. *Phys. Rev. Lett.*, 123:103201, 2019. doi:10.1103/PhysRevLett.123.103201.

[22] D. J. Wineland, C. Monroe, W. M. Itano, et al. Experimental issues in coherent quantum-state manipulation of trapped atomic ions. *Journal of research of the National Institute of Standards and Technology*, 103(3):259–328, 1998. doi:10.6028/jres.103.019.

[23] M. NIEMANN, A.-G. PASCHKE, T. DUBIELZIG, S. ULMER, and C. OSPELKAUS. *CPT TEST WITH (ANTI)PROTON MAGNETIC MOMENTS BASED ON QUANTUM LOGIC COOLING AND READ-OUT*, pages 41–44. doi:10.1142/9789814566438˙0011. URL `https://www.worldscientific.com/doi/abs/10.1142/9789814566438_0011`.

[24] A. Egl, I. Arapoglou, M. Höcker, et al. Application of the continuous Stern-Gerlach effect for laser spectroscopy of the $^{40}Ar^{13+}$ fine structure in a Penning trap. *Phys. Rev. Lett.*, 123:123001, 2019. doi:10.1103/PhysRevLett.123.123001.

[25] P. Micke, T. Leopold, S. A. King, et al. Coherent laser spectroscopy of highly charged ions using quantum logic. *Nature*, 578(7793):60–65, 2020. doi:10.1038/s41586-020-1959-8.

[26] M. J. Gutiérrez, J. Berrocal, F. Domínguez, et al. Dynamics of an unbalanced two-ion crystal in a Penning trap for application in optical mass spectrometry. *Phys. Rev. A*, 100:063415, 2019. doi:10.1103/PhysRevA.100.063415.

[27] L. S. Brown and G. Gabrielse. Geonium theory: Physics of a single electron or ion in a Penning trap. *Rev. Mod. Phys.*, 58:233–311, 1986. doi:10.1103/RevModPhys.58.233.

[28] H. Nagahama, G. Schneider, A. Mooser, et al. Highly sensitive superconducting circuits at 700 kHz with tunable quality factors for image-current detection of single trapped antiprotons. *Review of Scientific Instruments*, 87(11):113305, 2016. doi:10.1063/1.4967493.

[29] D. J. Wineland and H. G. Dehmelt. Principles of the stored ion calorimeter. *Journal of Applied Physics*, 46 (2):919–930, 1975. doi:10.1063/1.321602.

[30] E. A. Cornell, R. M. Weisskoff, K. R. Boyce, and D. E. Pritchard. Mode coupling in a Penning trap: π pulses and a classical avoided crossing. *Phys. Rev. A*, 41:312–

315, 1990. doi:10.1103/PhysRevA.41.312.

[31] H. Dehmelt. Continuous Stern-Gerlach effect: principle and idealized apparatus. *Proceedings of the National Academy of Sciences*, 83(8):2291–2294, 1986.

[32] W. M. Itano and D. J. Wineland. Laser cooling of ions stored in harmonic and Penning traps. *Phys. Rev. A*, 25: 35–54, 1982. doi:10.1103/PhysRevA.25.35.

[33] G. Gabrielse, L. Haarsma, and S. L. Rolston. Open-endcap Penning traps for high precision experiments. *International Journal of Mass Spectrometry and Ion Processes*, 88(2):319 – 332, 1989. ISSN 0168-1176. doi: https://doi.org/10.1016/0168-1176(89)85027-X.

[34] J. Ketter, T. Eronen, M. Höcker, S. Streubel, and K. Blaum. First-order perturbative calculation of the frequency-shifts caused by static cylindrically-symmetric electric and magnetic imperfections of a Penning trap. *International Journal of Mass Spectrometry*, 358:1 – 16, 2014. ISSN 1387-3806. doi: https://doi.org/10.1016/j.ijms.2013.10.005.

[35] N. Daniilidis and H. Häffner. Quantum interfaces between atomic and solid-state systems. *Annual Review of Condensed Matter Physics*, 4(1):83–112, 2013. doi: 10.1146/annurev-conmatphys-030212-184253.

[36] Sönke Alexander Möller. *How to couple trapped ions to superconducting resonators: towards hybrid quantum devices*. PhD thesis, University of California, Berkeley, 2016.

[37] B. Tu, F. Hahne, I. Arapoglou, et al. Tank-circuit assisted coupling method for sympathetic laser cooling. *Advanced Quantum Technologies*, 2021, accepted.

[38] A. Schneider, A. Mooser, A. Rischka, et al. A novel Penning-trap design for the high-precision measurement of the $^3He^{2+}$ nuclear magnetic moment. *Annalen der Physik*, 531:1800485, 2019. doi:10.1002/andp.201800485.

[39] F. Heiße, F. Köhler-Langes, S. Rau, et al. High-precision measurement of the proton's atomic mass. *Phys. Rev. Lett.*, 119:033001, 2017. doi: 10.1103/PhysRevLett.119.033001.

[40] J. A. Smith, S. Hamzeloui, D. J. Fink, and E. G. Myers. Rotational energy as mass in $H_3{}^+$ and lower limits on the atomic masses of d and ^{3}He. *Phys. Rev. Lett.*, 120: 143002, 2018. doi:10.1103/PhysRevLett.120.143002.

[41] S. Rau, F. Heiße, F. Köhler-Langes, et al. Penning trap mass measurements of the deuteron and the HD+ molecular ion. *Nature*, 585(7823):43–47, 2020. doi: 10.1038/s41586-020-2628-7.

[42] W. B. Cairncross, D. N. Gresh, M. Grau, et al. Precision measurement of the electron's electric dipole moment using trapped molecular ions. *Phys. Rev. Lett.*, 119:153001, 2017. doi:10.1103/PhysRevLett.119.153001.

[43] T. S. Roussy, D. A. Palken, W. B. Cairncross, et al. Experimental constraint on axion-like particle coupling over seven orders of magnitude in mass, 2020. URL `arxiv.org/abs/2006.15787`.

[44] X. Feng, M. Charlton, M Holzscheiter, R.A. Lewis, and Y. Yamazaki. Tank circuit model applied to particles in a Penning trap. *Journal of Applied Physics*, 79:8 – 13, 1996. doi:10.1063/1.360947.

[45] E. Zeuthen. Extending cavity-mechanical cooling via a hot LC electrical circuit framework for electromechanical coupling calculations. Master's thesis, The Niels Bohr Institute University of Copenhagen, 2012.

[46] M. Bohman. *Sympathetic Cooling of a Proton with Resonant Image Current Coupling*. PhD thesis, Ruperto-Carola University of Heidelberg, 2020.

[47] R Core Team. *R: A Language and Environment for Statistical Computing*. R Foundation for Statistical Computing, Vienna, Austria, 2020. URL `https://www.R-project.org/`.

[48] D. Eddelbuettel and R. François. Rcpp: Seamless R and C++ integration. *Journal of Statistical Software*, 40(8): 1–18, 2011. doi:10.18637/jss.v040.i08.

[49] H. Yoshida. Construction of higher order symplectic integrators. *Physics Letters A*, 150(5):262 – 268, 1990. ISSN 0375-9601. doi:https://doi.org/10.1016/0375-9601(90)90092-3.

[50] M. J. Borchert, P. E. Blessing, J. A. Devlin, et al. Measurement of ultralow heating rates of a single antiproton in a cryogenic Penning trap. *Phys. Rev. Lett.*, 122: 043201, 2019. doi:10.1103/PhysRevLett.122.043201.

Figures

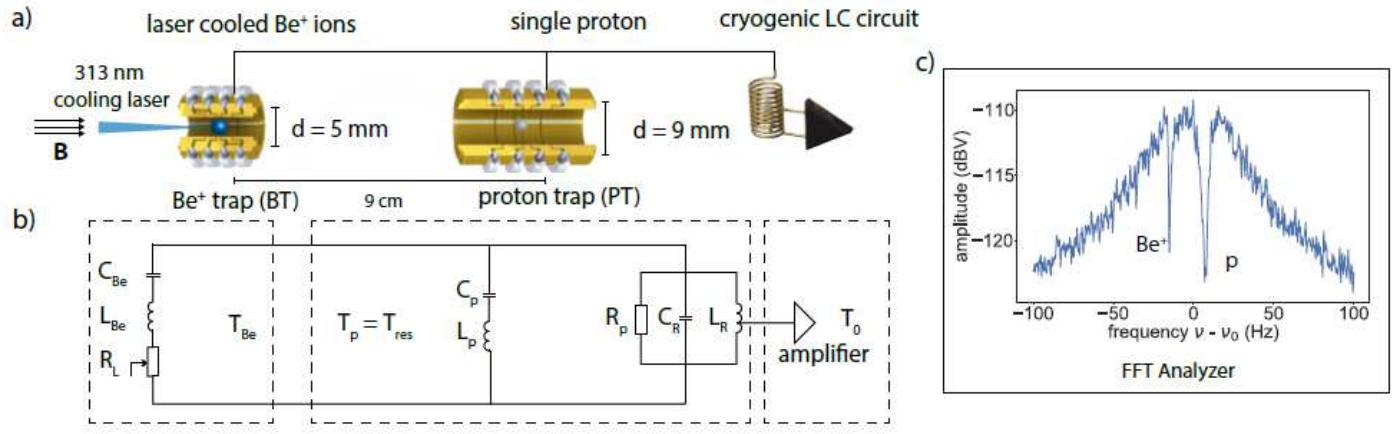

Figure 1

1: a) A single proton is stored in the proton trap (PT) while one or more Be+ ion(s) are stored in the beryllium trap (BT). The two ion traps, with inner diameters d = 9mm and d = 5mm, respectively, are connected to a cryogenic LC circuit with resonance frequency near their axial frequencies. One end of the resonance circuit is connected to a cryogenic amplier while the other is connected to rf ground. b) This system is described by a three part equivalent circuit, two series LC-circuits representing the trapped particles, and the LC-resonator with effective parallel resistance Rp as parallel RLC-circuit. The amplier is used to read out the image-current signal of the circuit, and drives the system with voltage noise at an effective temperature T0. c) The resulting FFT spectrum consists of the broad resonance of the detector (40 Hz FWHM) and two narrow \dips" (0:8 Hz FWHM for a single Be+ ion and 2:6 Hz FWHM for the proton) at the axial oscillation frequencies of the two trapped-ion systems.

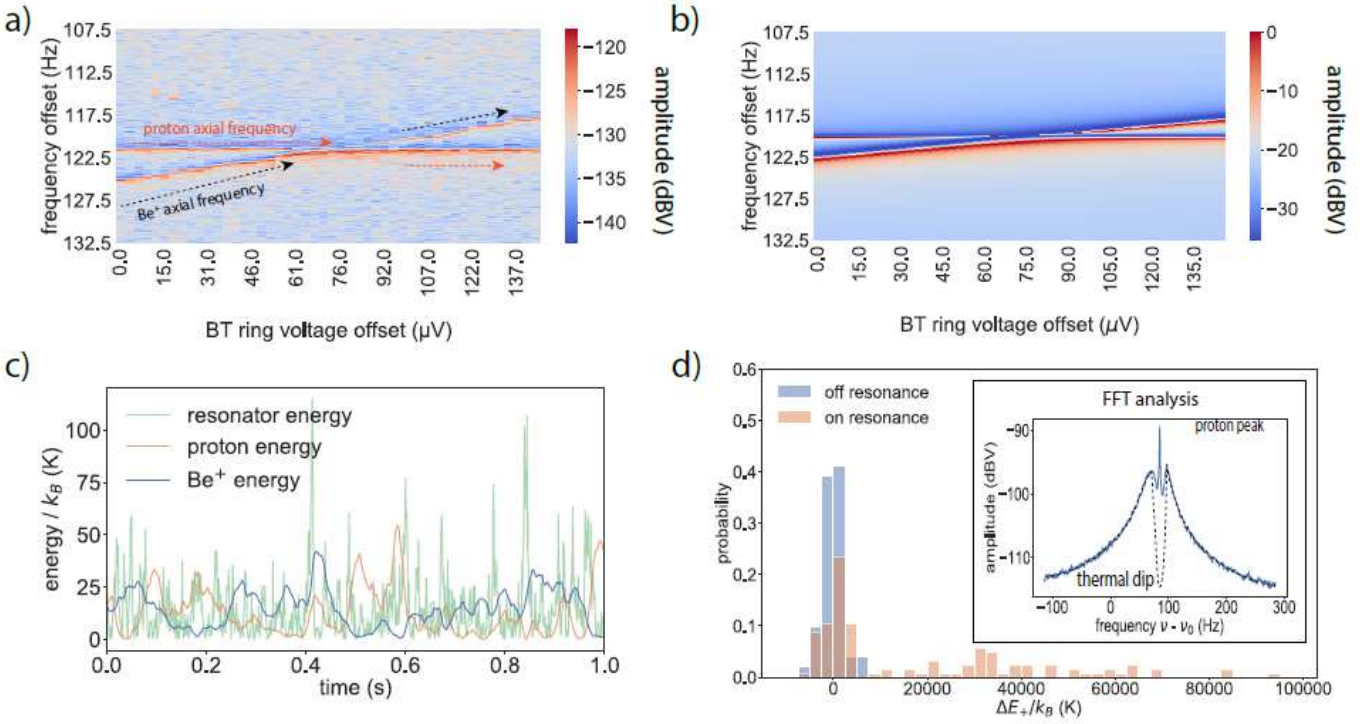

Figure 2

a) Measured FFT spectra of a single Be+ ion and the proton are presented as vertical cuts of the heatmap. The axial frequency of the proton is xed and the ring voltage of the BT trapping potential is scanned one step upwards after each FFT is recorded. b) The noise spectra expected from the impedance Z(v) of the equivalent circuit in Fig: 1 b) are presented in the same way as in a) and are calculated using the same parameters as in the experiment. c) An example of the energy exchange between the three oscillators at the resonance frequency of the LC circuit is simulated and includes the energy fluctuations from environment noise of the system. The energy of each oscillator depends on the phase relation with the environment noise so the time series shown here is one of infinitely many that could produce an FFT spectrum used in Fig: 2a). d) The change in axial energy of the proton after coupling to the rf-excited Be+ ions is shown when the Be+ ions are tuned away from resonance (blue) and tuned to resonance (orange). In both cases the excitation drive is present but only excites the proton via the resonant Be+ ions. A typical FFT spectrum (inset) shows the excited proton which appears as a narrow peak on top of the resonator and the Be+ dip which has reduced signal-to-noise compared to thermal equilibrium.

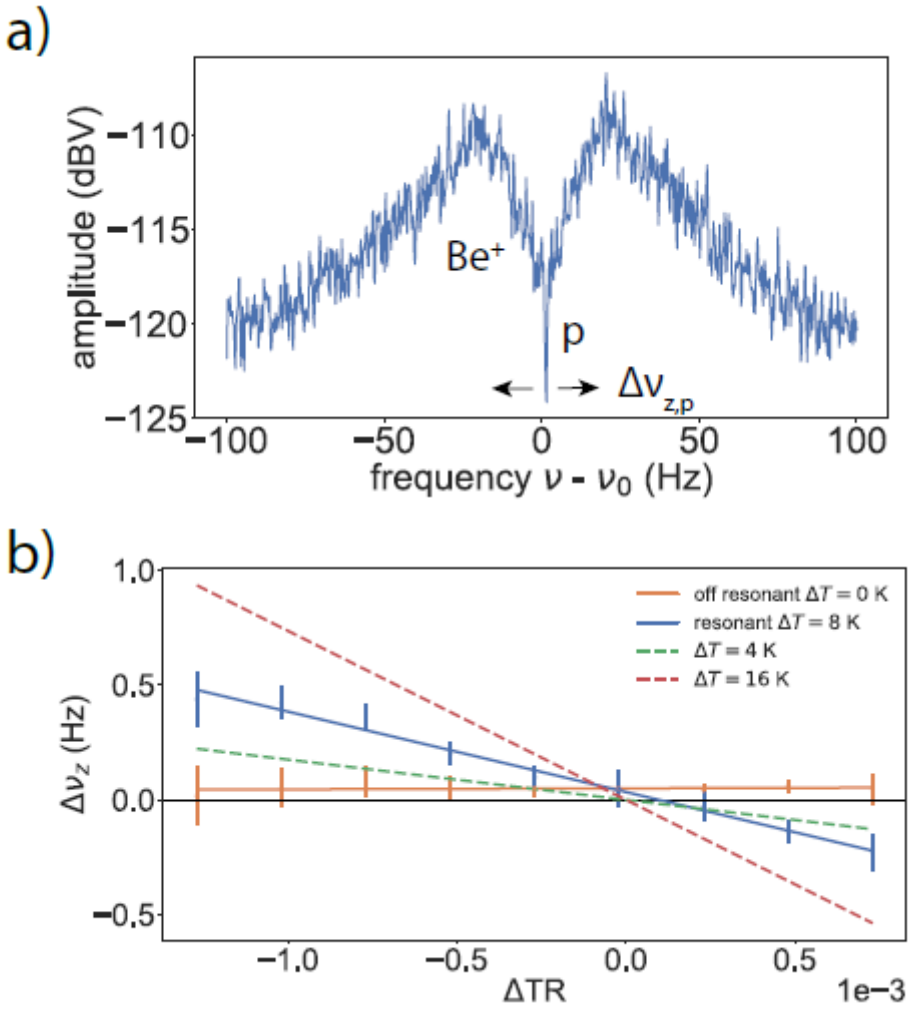

Figure 3

Please see the Manuscript PDF file for the complete figure caption.

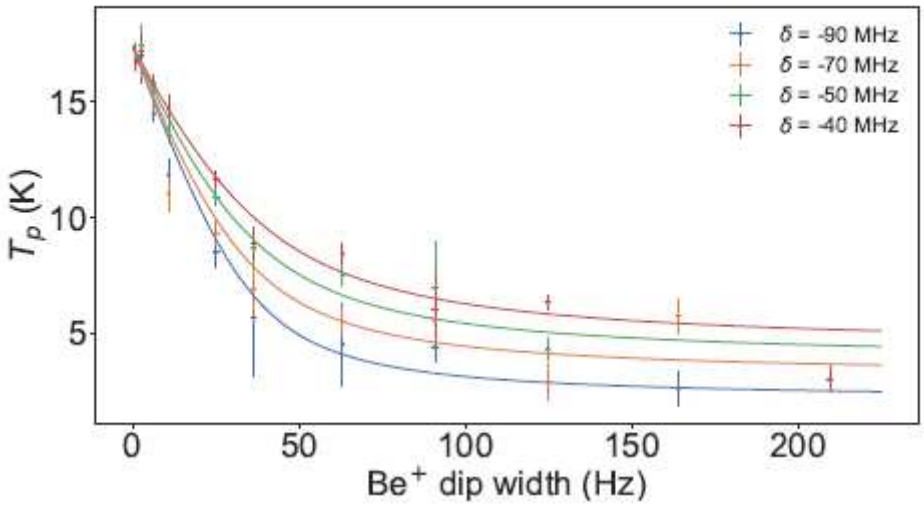

Figure 4

Please see the Manuscript PDF file for the complete figure caption.

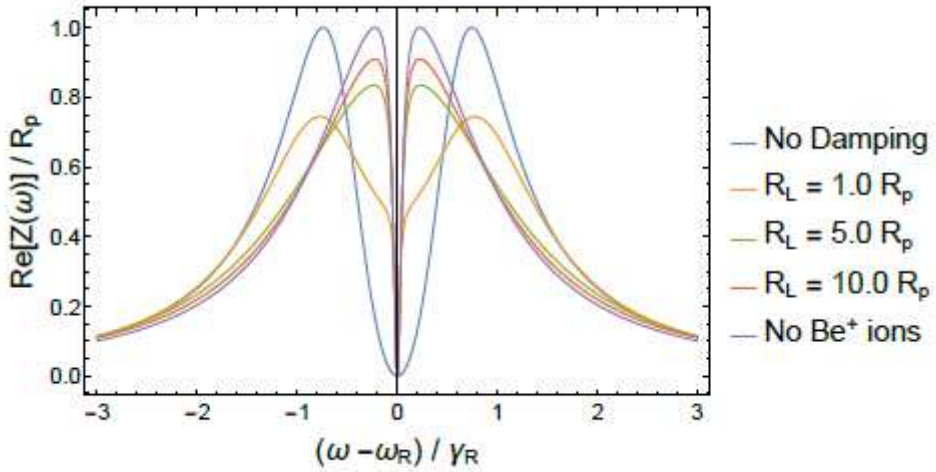

Figure 5

Please see the Manuscript PDF file for the complete figure caption.

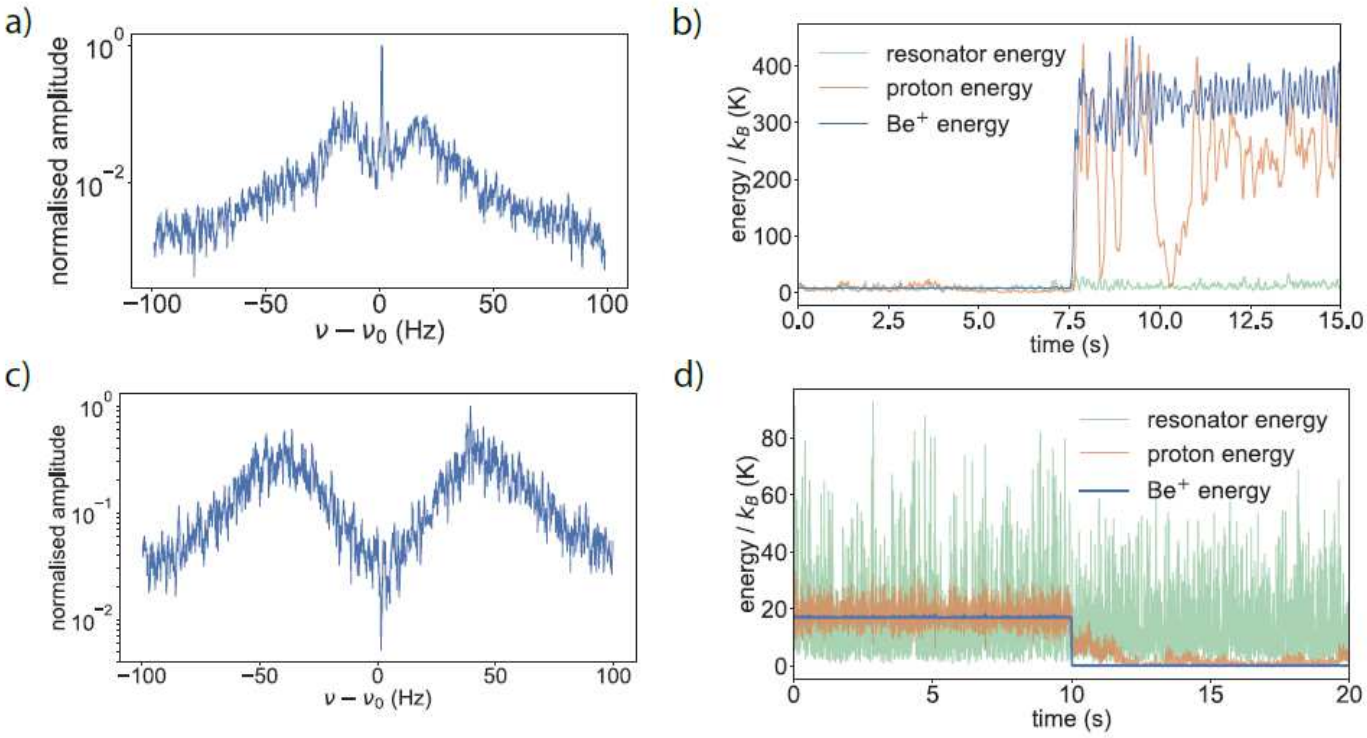

Figure 6

Computed FFT spectra are given in a) and c) to compare to the experimental results presented in the inset of Fig: 2 d) and Fig: 3 a) in the main text, respectively. In c) and d), we show representative time domain behaviour during heating and cooling measurements where the excitation drive or cooling laser is applied at times t = 7:5 s and t = 10 s, respectively.